# Seismic vulnerability analysis of reinforced concrete frame with infill walls considering in-plane and out-of-plane interactions

Dan Wang

*School of Civil Engineering, Northeast Forestry University, Harbin 150040, China*
*www_daa@163.com*

**ABSTRACT.** The seismic performance of a building hinges on the seismic capacity and damage features of the reinforced concrete (RC) frame with masonry infill walls. To reasonably evaluate the seismic performance and seismic economic loss of masonry infill walls, it is necessary to consider the in-plane (IP) and out-of-plane (OOP) interactions of these walls under seismic actions, and to model the vulnerability of the infill walls and the frame. Based on the test data on masonry infill walls, this paper designs a performance indicator for infill wall in the light of IP-OOP interactions, and determines the response threshold of each damage state. With the aid of OpenSees, the authors developed and verified a reasonable modeling method for RC frames with infill walls. As per the current code in China, a 5-storey RC frame with infill walls was designed, and two three-dimensional (3D) space models were established for the structure by the proposed modeling method. One of them considers IP-OOP interactions, and the other does not. Then, the structure was subjected to incremental dynamic analyses (IDA), and different damage indicators were determined to examine the damage of the infill walls and the overall structure, producing a set of vulnerability curves. The results show that the consideration of IP-OOP interactions significantly increases the probability of seismic damages on the infill walls and the overall structure. The most prominent increase was observed in the medium to serious damage stages.

**KEYWORDS.** Masonry infill walls; Reinforced concrete (RC) frame; In-plane (IP) and out-of-plane (OOP) interactions; Damage indicators; Seismic vulnerability analysis.

# INTRODUCTION

Each building is consisted of structural and non-structural components. The seismic performance of non-structural components is critical to the ductility of the building under earthquakes. As the most common non-structural components, infill walls are widely applied in reinforced concrete (RC) buildings. The data on the past earthquakes have shown that destruction of masonry infill walls will cause huge economic losses, and even endanger

human lives. In the structural seismic system, the seismic performance of the local components and overall structure depends on how well the infill walls contribute to stiffness and bearing capacity. In fact, the degree of damage for infill walls provides an important basis for evaluating the capacity of the building to prevent disasters before earthquakes, and assessing the possibility of continued use of the structure after earthquakes. Nevertheless, the existing studies on seismic design often ignore the role of masonry walls.

In the last decades, some researchers have tested the in-plane (IP) and out-of-plane (OOP) seismic performance of infill walls [1-6]. But only a few have investigated the IP and OOP interactions of masonry walls. The damage types observed in masonry infill walls are mainly divided into IP and OOP damages, and the damage usually stems from the interaction between IP and OOP. The previous results show that the IP and OOP interaction can reduce the strength and stiffness of the infill walls [7-9]. However, the nonlinear analyses on infill walls tend to focus on the IP behavior, failing to consider its interaction with OOP behavior.

The performance indicator of masonry infill wall largely reflects the severity of wall damages, revealing the macro damage states. In current studies, the vulnerability of masonry infill walls is mainly examined with the interlayer displacement angle as the IP indicator, before plotting the vulnerability curve. Based on the description of macro damage phenomena, Chiozzi et al. [10] defined the damage states for establishing the vulnerability curve. The specific description of each damage state in this standard is based on the collected test results. Tab. 1 reports three different macro descriptions for infill wall damage states, namely, slight damage (DS1), moderate damage (DS2), and severe damage (DS3), and the corresponding repair measures. Cardone et al. [11] and Sassun et al. [12] adopted similar macro descriptions of the damage state, determined the interlayer displacement angle when each specimen reached a certain damage state, and established the IP vulnerability function of masonry infill walls. The vulnerability curves of infill walls, which display the probability distribution of different interlayer displacement angles, only consider the damage indicator in a single direction, and could not reflect the influence of OOP damage under earthquake action on the vulnerability of infill walls.

| Degree of damage | Macro description | Limit of crack width | Repair measure |
| --- | --- | --- | --- |
| DS1 | Very slight cracks appear at mortar joints, decorative surface, or the wall-frame junction. There is no obvious slip crack or crushed block. | 1mm | Reapply plaster to cover visible cracks. |
| DS2 | Obvious diagonal cracks appear at mortar joints or blocks. There may be slippage along brickwork joints, or local crushing of blocks. | 2mm | Repair the cracks through pressure grouting, or rebuild locally broken masonry, and reapply high-quality plaster to the surface. |
| DS3 | Wide oblique cracks appear, exposing the opposite surface. There are obvious mortar cracks, and wide crushing, extrusion, and spalling of blocks. | 4mm | Demolish and rebuild the entire structure. |

Table 1: Judgement criteria and repair measures for damage states of masonry infill walls.

Following various mechanical approaches, new simplified models have been developed to predict both IP and OOP responses, with the aim of simulating the exact response of structures with infill walls. The accurate calibration of infill wall simulation models requires massive data from tests with both IP and OOP loads. Due to the severe lack of such data, most macroscale models for the OOP responses, and IP-OOP interactions of infill walls are grounded loosely on simplified hypotheses. Kadysiewski et al. [13] proposed an infill wall model, which considers the IP-OOP interactions with two diagonal beam-column elements, and a lumped mass of the central node, and put forward the interaction curves for IP and OOP displacements. On this basis, Furtado et al. [14] established a simplified infill wall model with four beam-column elements, two OOP lumped masses, and a central element, before introducing the law of lag to simulate the strength and stiffness degradation of masonry infill wall.

Based on the test data of frames with masonry infill walls, this paper firstly defines a quantitative indicator considering the coupling between IP and OOP damages of infill walls, and determines the indicator limit at each damage state. Next, a simplified model was introduced for the RC frame with infill walls, which is capable of simulating IP-OOP interactions, and a nonlinear analysis model of infill-wall RC frame was established with the help of OpenSees. The accuracy of the

model was verified through the numerical simulation of an infilled RC frame in the quasi-static test. Then, a 5-storey infill-wall RC frame was designed using PKPM, and two 3D space models were established for the structure, with and without IP-OOP interactions, respectively. A total of 20 ground motion records were selected to conduct an incremental dynamic analysis (IDA) on the prepared structure. On this basis, the seismic vulnerability of the infill walls and the overall structure was explored in details, a set of vulnerability curves considering IP-OOP interactions was proposed tentatively, which illustrate the probability of exceedance of the infill walls and the overall structure at different performance levels, as a function of the seismic intensity.

## DAMAGE INDICATOR IDENTIFICATION

### Response thresholds

To design the damage indicator for infill walls, it is important to gather statistical information about the level of deformation corresponding to each damage state. Hence, the authors collected the results of the IP and OOP quasi-static loading tests on 30 RC frames with masonry infill walls [1-7, 9]. According to the descriptions of the damage phenomena of each frame under load, the response thresholds of IP and OOP frames were recorded under each damage state. As for the quantification indicators of infill wall damages, the interlayer displacement angle $\Delta_{IP0}/H$ was chosen for the IP scenario, while the ratio $\Delta_{OOP0}/H$ of the maximum OOP displacement to the distance between the top beam axis and the upper edge of the grade beam was selected for the OOP scenario.
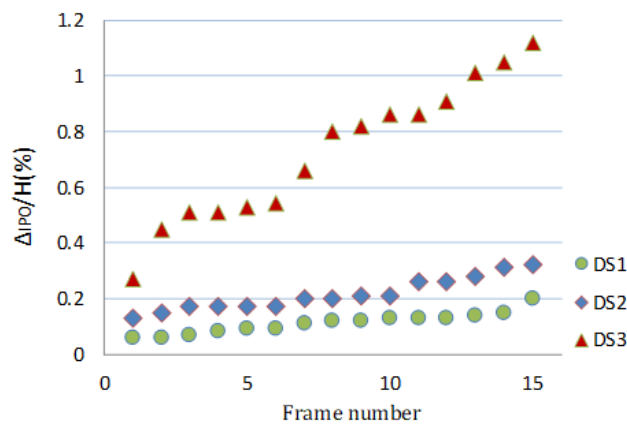


Figure 1: Response thresholds of each IP frame in different damage states
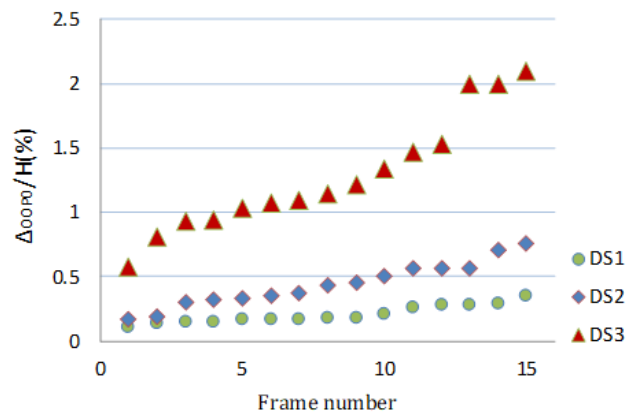


Figure 2: Response thresholds of each OOP frame in different damage states

As shown in Figs. 1 and 2, the response thresholds of the specimens reflect a certain discreteness. To determine the quantification indicators for the RC frames with infill walls in each damage state, the demand parameter was calculated by the vulnerability analysis approach in the appendix of FEMA P-58 [15].

In general, the vulnerability function obeys the log normal distribution:

$$P(D) = \Phi \left[ \frac{\ln\left(\dfrac{D}{\theta}\right)}{\beta} \right] \tag{1}$$

where, $P(D)$ is the probability to reach or exceed a damage state; $\Phi$ is the cumulative function of standard normal distribution; $\theta$ is the mean of engineering demand parameter D; $\beta$ is the log standard deviation reflecting the discreteness of D.

If the frame data come from multiple independent tests and record the D of each frame in each damage state, then the demand parameter $\theta$ can be calculated by:

$$\theta_i = e^{\left(\frac{1}{N}\sum_{j=1}^{N}\ln d_j\right)} \tag{2}$$

where, $\theta_i$ is the demand parameter of damage state i; N is the number of frames; $d_j$ is the response threshold for the j-th frame in damage state i.

The calculated demand parameters of IP and OOP frames are the response thresholds of infill walls at each damage state under IP and OOP scenarios (Tab. 2).

| Type | Performance indicator | DS1 | DS2 | DS3 |
|------|----------------------|------|------|------|
| IP | $\Delta_{IP0}/H$ (%) | 0.11 | 0.20 | 0.68 |
| OOP | $\Delta_{OOP0}/H$ (%) | 0.20 | 0.40 | 1.21 |

Table 2: Response thresholds of infill walls at each damage state under IP and OOP scenarios

*Performance indicator*

*IP-OOP interactions.* In 2007, Hashemi and Mosalam relied on the strut-and-tie (SAT) model to prove that the IP strength of infill walls interact with their OOP strength. Later, a series of tests and numerical simulations were carried out, revealing that the simulation effect agrees well with the test results, when the interactive effect is described as the curve in Fig. 3(a):

$$\left(\frac{P_H}{P_{H0}}\right)^{3/2} + \left(\frac{M_N}{M_{N0}}\right)^{3/2} \leq 1.0 \tag{3}$$

where, $P_H$ and $P_{H0}$ are the IP forces in the presence and absence of OOP force, respectively; $M_N$ and $M_{N0}$ are the OOP forces in the presence and absence of IP force, respectively.

Mosalam and Günay [16] depicted the displacement interaction with the same equations for force interaction. In the elastic stage, the displacement interaction satisfies the 2/3 power curve formula, for the elastic displacement is positively proportional to the load. As shown in Fig. 3, the non-elastic displacement could be approximated by the 3/2 power curve. The interactive relationship between IP and OOP displacements can be expressed as:

$$\left(\frac{\Delta_H}{\Delta_{Hy0}}\right)^{3/2} + \left(\frac{\Delta_N}{\Delta_{Ny0}}\right)^{3/2} \leq 1.0 \tag{4}$$

where, $\Delta_H$ is the IP horizontal displacement of infill wall; $\Delta_{Hy0}$ is the IP horizontal displacement in the absence of OOP force; $\Delta_N$ is the OOP horizontal displacement of infill wall; $\Delta_{Ny0}$ is the OOP horizontal displacement in the absence of IP force.



(a) Force interaction curve of an infill wall       (b) Displacement interaction curve of an infill wall
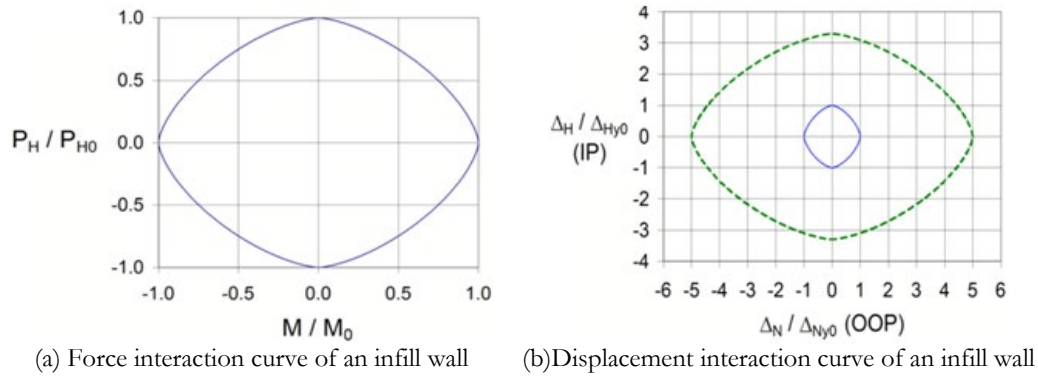
Figure 3: IP-OOP interactions of an infill wall

*Performance indicator and response thresholds.* Substituting $\Delta_{H0}$ and $\Delta_{Hy0}$, which respectively correspond to IP and OOP response thresholds into formula (4), the interactive relationships between IP and OOP displacements under the three limit states can be respectively obtained by:

$$\left(\frac{\Delta_{IP1}/H}{0.0011}\right)^{3/2} + \left(\frac{\Delta_{OOP1}/H}{0.0020}\right)^{3/2} = 1.0 \tag{5}$$

$$\left(\frac{\Delta_{IP2}/H}{0.0020}\right)^{3/2} + \left(\frac{\Delta_{OOP2}/H}{0.0040}\right)^{3/2} = 1.0 \tag{6}$$

$$\left(\frac{\Delta_{IP3}/H}{0.0068}\right)^{3/2} + \left(\frac{\Delta_{OOP3}/H}{0.0121}\right)^{3/2} = 1.0 \tag{7}$$

where, $\Delta_{IPi}$ and $\Delta_{OOPi}$ are the IP horizontal displacement and OOP horizontal displacement of infill walls in damage state DSi under the joint action of IP and OOP forces, respectively.

The relationships between IP and OOP displacements under the three limit states can be respectively calculated by:

$$2.45\left(\frac{\Delta_{IP1}}{H}\right)^{3/2} + \left(\frac{\Delta_{OOP1}}{H}\right)^{3/2} = 8.94 \times 10^{-5} \tag{8}$$

$$2.83\left(\frac{\Delta_{IP2}}{H}\right)^{3/2} + \left(\frac{\Delta_{OOP2}}{H}\right)^{3/2} = 2.53 \times 10^{-4} \tag{9}$$

$$2.54\left(\frac{\Delta_{IP3}}{H}\right)^{3/2} + \left(\frac{\Delta_{OOP3}}{H}\right)^{3/2} = 1.33 \times 10^{-3} \tag{10}$$

The coefficient values of $\left(\frac{\Delta_{IPi}}{H}\right)^{3/2}$ are similar in the above formulas. The arithmetic mean was taken as the coefficient of $\left(\frac{\Delta_{IPi}}{H}\right)^{3/2}$. That is, the sum of $2.6\left(\frac{\Delta_{IP}}{H}\right)^{3/2} + \left(\frac{\Delta_{OOP}}{H}\right)^{3/2}$ was adopted as the quantification indicator of IP-OOP interactions for infill walls. Then, the response thresholds under different damage states can be obtained as shown in Tab. 3.

| Performance indicator | DS1 | DS2 | DS3 |
|---|---|---|---|
| $2.6\left(\dfrac{\Delta_{IP}}{H}\right)^{3/2}+\left(\dfrac{\Delta_{OOP}}{H}\right)^{3/2}$ | $8.94\times10^{-5}$ | $2.53\times10^{-4}$ | $1.33\times10^{-3}$ |

Table 3: Response thresholds of the IP-OOP interactions for infill walls under different damage states.

According to Xie's IP-OOP loading test data, three frames $T_1$, $T_2$ and $T_3$ were selected for verification. All three frames are full-scale RC frames with a single-layer, single-span hollow concrete block infill wall. Frame $T_1$ has been slightly damaged through IP loading, with an interlayer displacement angle of 0.15%. Without changing the IP displacement, the infill wall was applied a unidirectional IOP load until the bearing capacity significantly dropped. Then, the frame was adopted to verify the response thresholds under DS2 and DS3. Frames $T_2$ and $T_3$ have been moderately damaged through IP loading, with an interlayer displacement angle of 0.21% and 0.50%, respectively. These two frames were utilized to verify the response thresholds under DS3. Drawing on the frame damage phenomena in the literature, and the force-displacement skeleton curves of OOP loading, the response thresholds of each frame in different damage states were obtained under the joint action of IP and OOP forces, and compared with the calculation results in Tab. 3. The verification results of the three frames are shown in Tabs. 4 and 5.

| Damage state | DS2 | DS3 |
|---|---|---|
| $\Delta_{OOP}/H$ | 0.19% | 1.23% |
| $2.6\left(\dfrac{\Delta_{IP}}{H}\right)^{3/2}+\left(\dfrac{\Delta_{OOP}}{H}\right)^{3/2}$ | $2.33\times10^{-4}$ | $1.51\times10^{-3}$ |
| Preset response threshold | $2.53\times10^{-4}$ | $1.33\times10^{-3}$ |
| Error | 0.08 | 0.13 |

Table 4: Response thresholds of frame $T_1$ ($\Delta_{IP}/H$=0.15%) under the joint action of IP and OOP forces.

| Frame | $T_2$ | $T_3$ |
|---|---|---|
| $\Delta_{IP}/H$ | 0.21% | 0.50% |
| $\Delta_{OOP}/H$ | 0.89% | 0.81% |
| $2.6\left(\dfrac{\Delta_{IP}}{H}\right)^{3/2}+\left(\dfrac{\Delta_{OOP}}{H}\right)^{3/2}$ | $1.09\times10^{-3}$ | $1.63\times10^{-3}$ |
| Preset response threshold | $1.33\times10^{-3}$ | $1.33\times10^{-3}$ |
| Error | 0.18 | 0.22 |

Table 5: Response thresholds of frames $T_2$ and $T_3$ in DS3 under the joint action of IP and OOP forces.

As shown in Figs. 1 and 2, the response thresholds of infill walls under different damage states were highly discrete. The highest discreteness appeared in DS3. Cardone et al. summarized the response thresholds of IP interlayer displacement angle for infill walls in different damage states, and found that the log standard deviation under different damage states falls between 0.18 and 0.45. Therefore, the errors (0.08-0.22) in Tabs. 4 and 5 were relatively small. Thus, the performance indicator and thresholds in Tab. 3 were selected for the IP-OOP interactions of infill walls.

*Damage indicators and limit states.* According to the above results, the performance levels of infill walls can be defined by the IP-OOP indicator and the IP indicator, as shown in Tab. 6.

Rosseto et al. [17] proposed a damage indicator based on the maximum interlayer displacement angle. This indicator applies to the performance level of structures with different lateral stiffnesses. Using this indicator, the RC frame with infill wall was divided into 5 damage states (Tab. 7).

| Degree of damage | Macro description | Limit value of each indicator | |
|---|---|---|---|
| | | $2.6\left(\dfrac{\Delta_{IP}}{H}\right)^{3/2}+\left(\dfrac{\Delta_{OOP}}{H}\right)^{3/2}$ | $\Delta_{IP0}/H.$ |
| DS1 | Very slight cracks appear at mortar joints, decorative surface, or the wall-frame junction. There is no obvious slip crack or crushed block. | $8.94\times10^{-5}$ | $1.10\times10^{-3}$ |
| DS2 | Obvious diagonal cracks appear at mortar joints or blocks. There may be slippage along brickwork joints, or local crushing of blocks. | $2.53\times10^{-4}$ | $2.00\times10^{-3}$ |
| DS3 | Wide oblique cracks appear, exposing the opposite surface. There are obvious mortar cracks, and wide crushing, extrusion, and spalling of blocks. | $1.33\times10^{-3}$ | $6.80\times10^{-3}$ |

Table 6: Performance levels of masonry infill walls.

| Damage state | Macro description | Maximum interlayer displacement angle $\theta_{max}$ (%) |
|---|---|---|
| Near intactness (DS1) | Very slight cracks appear on infill wall. | 0.05 |
| Slight damage (DS2) | Blocks at beam-column junctions are crushed, the structural elements are initially damages, and the infill wall of external frame suffers from diagonal shear cracking. | 0.30 |
| Moderate damage (DS3) | Wide cracking hits infill wall. The blocks suffer from crushing or OOP extruding. Infill wall partially fails. The structural elements are further damaged, with shear damages in local areas. | 1.15 |
| Partial collapse (DS4) | Partial collapse occurs due to the damages of the beams and columns. Infill wall almost fully fails. | 2.80 |
| Collapse (DS5) | Infill wall suffers obvious overall collapse. | 4.40 |

Table 7: Performance levels of RC frame with infill walls.

## NUMERICAL SIMULATION

### *Infill wall model*

Furtado et al. [14] modelled an infill wall of four elastic beam elements, two OOP lump masses, and one nonlinear axial connection element (Fig. 4). The model can simulate the behavior of infill walls under cyclic IP and OOP loading, and realize the IP-OOP interactions by element removal.

*IP features.* As shown in Fig. 4, the central element of the model reflects the nonlinear stress-strain of the infill wall under cyclic IP loading. The force-displacement relationship of the central element was characterized by the performance skeleton curve of the infill wall (Fig. 5). Furtado provided the recommended values for the definition of the skeleton curve:

(1) The ratio of cracking strength to the maximum strength ($f_{i,c}/f_{i,max}$) is 0.55. According to the mechanical performance of masonry and mortar, the cracking displacement $d_{fi,c}$ falls between 0.075% and 0.12%.

(2) The yield strength $d_{i,y}$ and yield displacement $d_{fi,y}$ are defined as the midpoints of crack displacement coordinates ($d_{fi,c}/f_{i,c}$) and maximum strength displacement coordinates ($d_{fi,max}/f_{i,max}$), respeectively. The yield strength is 65%-75% of the maximum strength, while the yield displacement is between 0.15% and 0.35%.

(3) The maximum strength $f_{i,max}$ can be solved by:

$$F_{i,max} = 0.818\frac{l_i \times t_i \times f_{ms}}{C_I}\left(1+\sqrt{C_I^2+1}\right) \tag{11}$$

$$f_{i,\max} = 0.818 \frac{f_{ms}}{C_I}\left(1 + \sqrt{C_I^2 + 1}\right) \tag{12}$$

$$C_I = 1.925 \frac{l_i}{b_i} \tag{13}$$

where, $f_{ms}$ is the tested shear strength of masonry; $t_i$, $b_i$, and $l_i$ are the thickness, height, and length of the infill wall, respectively. The maximum strength displacement $d_{fi,max}$ is about 0.25%-0.5%.
(4) The displacement corresponding to the residual strength is 5 times the maximum strength displacement. The residual strength is around 20% of the maximum strength.
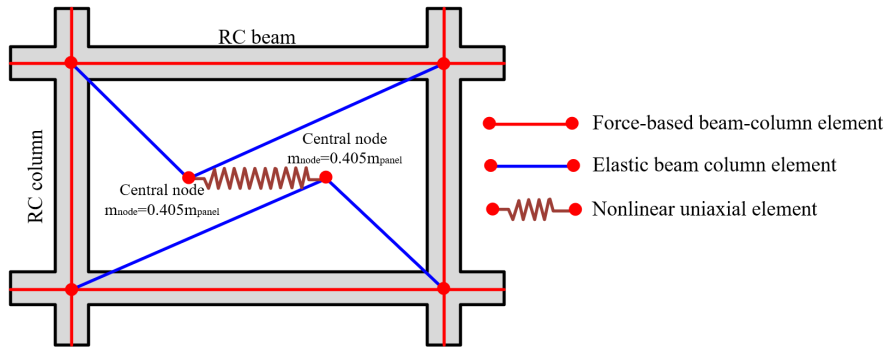


Figure 4: Furtado et al.'s model [14].
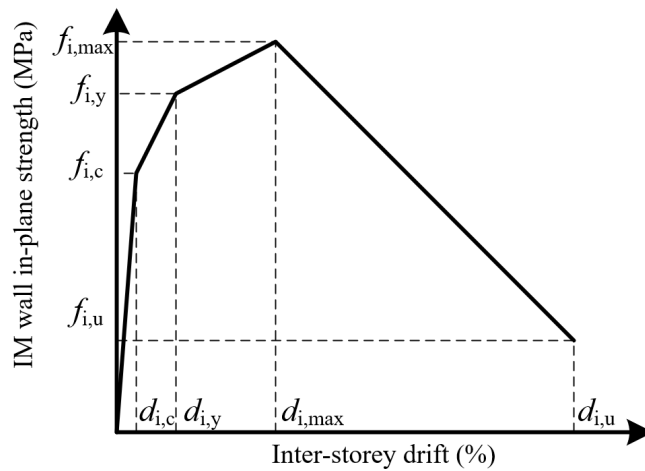


Figure 5: Skeleton curve of the infill wall.
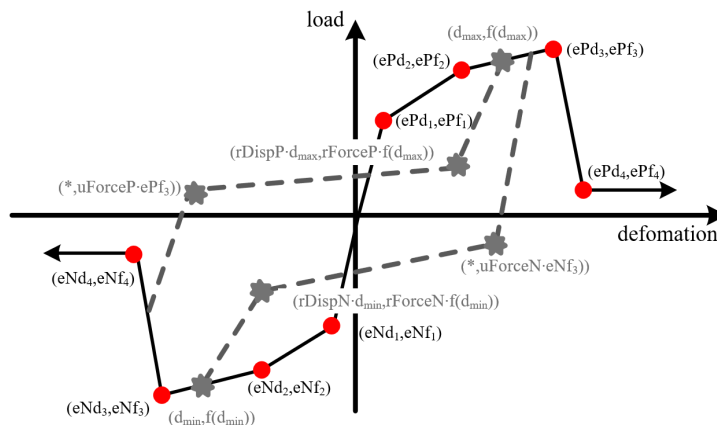


Figure 6: Response of Pinching4 uniaxial material model

For the central element, the Pinching4 uniaxial material model was adopted to describe the hysteresis mode of the infill wall. Noh and Huang [18, 19] demonstrated the high sensitivity of numerous Pinching4 material parameters, and proved their capability of simulating the extrusion load - deformation response, and representing the degradation mode under cyclic loading. The cyclic degradation of strength and stiffness occurs in three forms: unloading stiffness degradation, reloading stiffness degradation, and strength degradation. In the calibrated filling model, the hysteresis mode is controlled by additional parameters: stiffness degradation, strength degradation, shrinkage effect, and energy degradation. The skeleton curve and unloading-reloading path of the hysteresis mode in the model are displayed in Fig. 6.

*OOP features.* Drawing on the joint action between IP and OOP proposed by Kadysiewski and Mosalam [13], the Furtado model assumes that the OOP behavior of infill walls is linear and elastic, the model and infill walls have the same natural frequencies, and the IP is nonlinearly correlated with OOP. According to Kadysiewski and Mosalam, the OOP effective mass of an infill wall was calculated as 0.81M, where M is the total mass of the wall. The OOP lumped mass was evenly distributed to the two nodes of the central element. The equivalent strut width of the infill wall, and the equivalent inertial moment in the OOP direction can be respectively calculated by:

$$w = 0.175(\lambda h_{col})^{-0.4} d_i \tag{14}$$

$$\lambda = \left( \frac{E_i t_i \sin 2\theta}{4 E_c I_{col} h_i} \right)^{0.25} \tag{15}$$

$$d_i = \sqrt{h_i^2 + l_i^2} \tag{16}$$

$$I_{eq} = 1.644 \left( \frac{d_i}{h_i} \right)^3 \times I_i \tag{17}$$

where, $\lambda$ is the dimensionless parameter for the relative stiffness between the infill wall and the frame; $h_{col}$ is the layer height of the frame; $E_i$ and $E_c$ are the elastic moduli of the masonry, and the RC of the frame, respectively; $I_{col}$ is the effective cross-sectional inertial moment of the strut; $d_i$ is the diagonal length of the infill wall; $h_i$, $l_i$, and $t_i$ are the height, length, and thickness of the infill wall, respectively; $\theta$ is the angle between the diagonal and horizontal axis of the infill wall; $I_{eq}$ is the equivalent inertial moment of the infill wall; $I_i$ is the effective cross-sectional inertial moment of the infill wall.

Kadysiewski et al. proposed the element removal method for infill walls, aiming to simulate the seismic response of such walls more truthfully. The method assumes that any infill wall would collapse, once its displacement surpasses the limit range under the joint action of IP and OOP. Then, the mass and stiffness of the infill wall are automatically removed from the structure by the algorithm. In our Furtado model, the IP-OOP interaction zone of the infill wall has linear boundaries. For intact infill walls, the maximum IP and OOP displacement angles were set to 1.5% and 3%, respectively.

### RC frame model

This paper uses force-based nonlinear distribution elements to simulate the beam and column elements of the RC frame. The nonlinear deformation of beam and column elements was simulated by integrating the deformable region along the length on the cross-section of each element. The cross-section of each beam and column element was represented by discrete fibers, all of which obey the uniaxial stress-strain law. The bending state of the cross-section of each beam and column element was obtained by integrating the nonlinear uniaxial stress-strain response of each fiber on that cross-section.

To investigate the seismic response of the RC frame, it is necessary to consider the nonlinearity, i.e., the uniaxial stress-strain response of the material. Specifically, the Concrete 02 uniaxial material model of OpenSees was adopted as the constitutive model of concrete. The rebars were regarded as the Steel 02 uniaxial material, following the Giuffre-Menegotto-Pinto theory. The material has been applied to uniaxial material models with homogeneous strain hardening. Here, the strain hardening ratio is set to 1%. The three parameters of the command stream of the Steel 02 model, R0, R1 and R2, which control the rebars' transition from elastic state to plastic state, were set to 18, 0.925, and 0.15, respectively.

### Model calibration and validation

Model calibration was performed by comparing the numerical outputs to available Zhao's test results on the frame with

infill walls under IP-OOP loading. With a reduced scale of 1/2, the frame is an RC frame with a single-layer, single-span, non-hollow infill wall. Fig. 7 shows the dimensions and rebar arrangement of the frame. Tab. 8 lists the material properties.
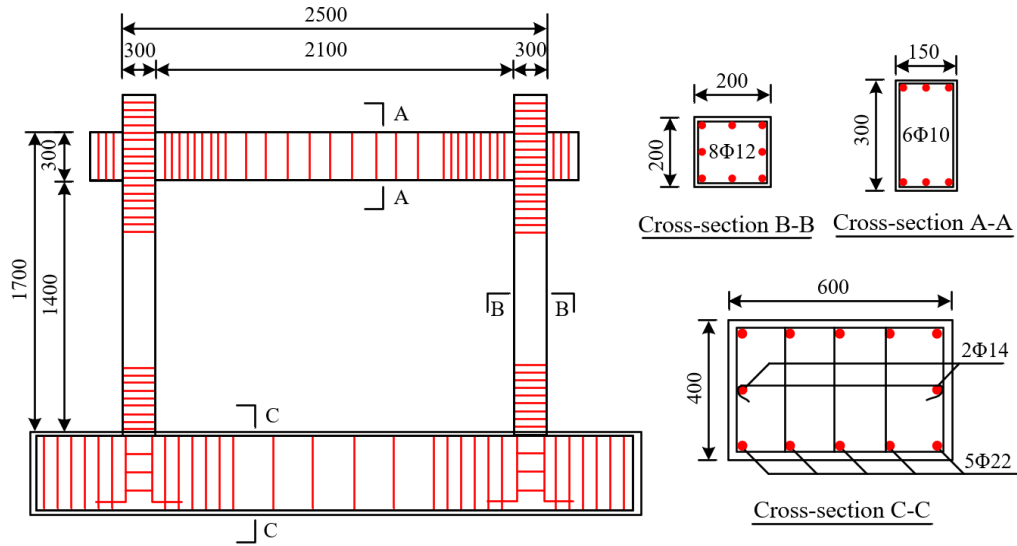


Figure 7: Dimensions and rebar arrange of the test frame

| Material | Mechanical property | Parameter value |
|---|---|---|
| Concrete | Compressive strength / Mpa | 37.46 |
| | Elastic modulus / GPa | 29.50 |
| Rebar | Yield intensity / MPa | 447.70 |
| | Tensile strength / MPa | 659.13 |
| | Elastic modulus / GPa | 198.41 |
| Block | Compressive strength / MPa | 4.90 |
| Masonry | Compressive strength / MPa | 16.49 |
| | Shear strength / MPa | 0.31 |
| | Bulk density /kN/m³ | 5.80 |

Table 8: Material properties of the frame.
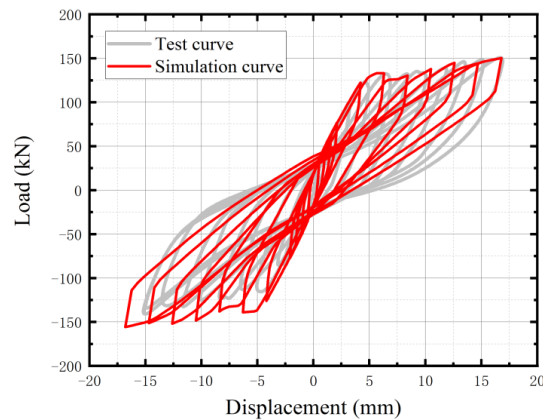


Figure 8: Simulated and test hysteresis curves.

According to the test information, the mechanical parameters of the infill wall were calculated. After loading, the model was subjected to IP-OOP loading. Fig. 8 compares the simulated hysteresis curve with the test data. Fig. 9 compares the simulated and test backbone curves. The simulation results basically agree with the test results.
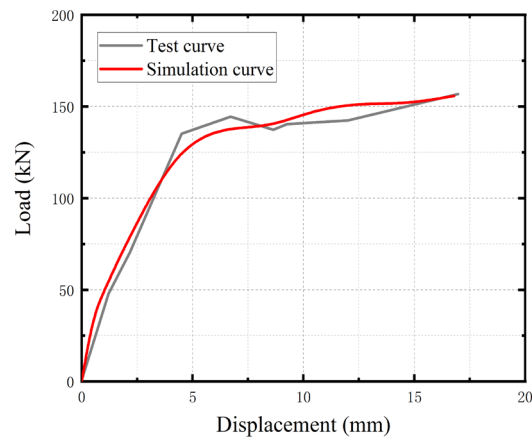
Figure 9: Simulated and test backbone curves.

Under IP-OOP loading, when the OOP displacement of the central element reached 15.50mm, the infill wall model reached the IP-OOP interactive boundary, and the wall failed. The result was close to the failure displacement (15.2mm) when the OOP loading stopped in the test. This proves that our model can approximate the deformation of the infill wall under OOP load. The comparison suggests that the proposed simplified model for the RC frame with infill walls, which considers IP-OOP interactions, can roughly simulate and verify the IP mechanical performance and OOP deformation capability of RC frames with infill walls, laying a solid basis for further analysis.

*Case building*

Referring to the *Code for Seismic Design of Buildings* (GB50011-2010), the PKPM software was adopted to design an RC frame, with a five-layered infill wall (6 spans in the X direction and 3 spans in the Y direction), as the analytical model. Fig. 10 shows the plane layout of the structure: the bottom layer is 4.2m tall, and the other layers are 3.6m tall. The concrete grade was set to C30. The horizontal load-bearing rebars are of the grade HRB400 with a diameter of 22 cm. The stirrups are of the grade HPB300. The infill wall was prepared from the clay brick blocks obtained through tests (thickness: 150 mm). The floor and roof slabs are both 100mm thick. The building and site belong to Class C and Class III, respectively. The designed earthquake group, and seismic fortification intensity were set to 2 and 8, respectively.

Following the above modelling strategy, two models were established for the above structure. One of the models considers the IP-OOP interactions of the infill wall (IP-OOP), and the other considers the IP force effect of the wall (IP). In the IP model, the infill wall was modelled without considering OOP bending stiffness and the mass of the central element. Tabs. 9-11 present the mechanical parameters of concrete, rebars, and infill wall in the structure, respectively.
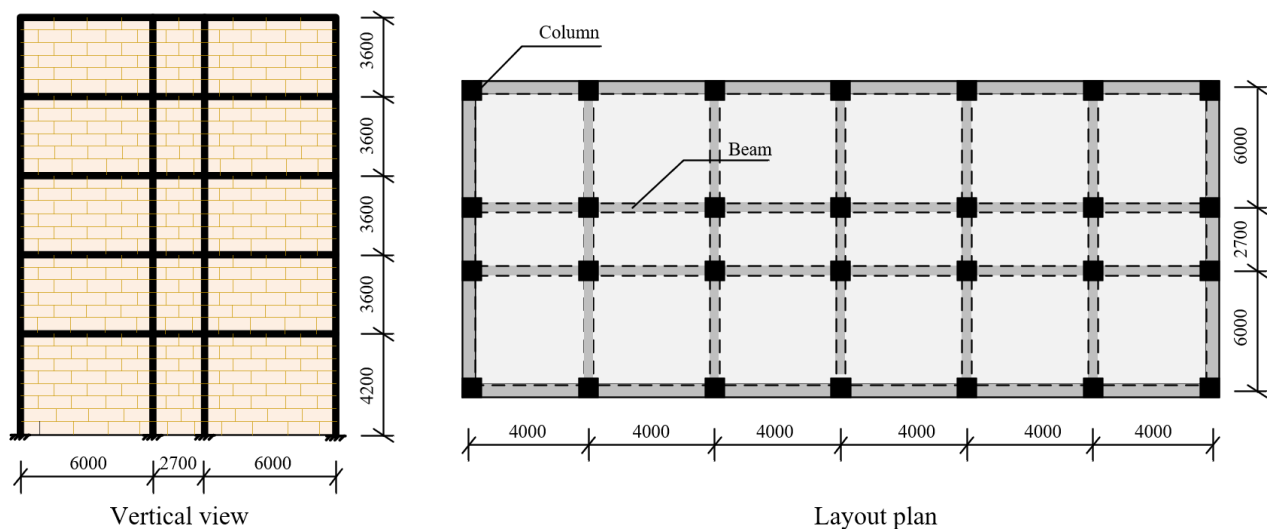


Figure 10: 3D spatial RC frame with infill wall.

| Grade | Peak stress (MPa) Compressive | Tensile | Peak strain | Ultimate stress (MPa) | Ultimate strain | Elastic modulus (MPa) |
|---|---|---|---|---|---|---|
| C30 | 28.72 | 2.87 | 0.0022 | 5.74 | 0.01 | 3236 |

Table 9: Mechanical parameters of concrete.

| Rebar grade | Yield strength (MPa) | Ultimate strain | Elastic modulus (GPa) |
|---|---|---|---|
| HRB400 | 445.50 | 0.01 | 200 |

Table 10: Mechanical parameters of rebars.

| Compressive strength (MPa) | Shear strength (MPa) | Elastic modulus (MPa) | Shear modulus (MPa) | Bulk density (kN/m³) |
|---|---|---|---|---|
| 2.02 | 0.55 | 1873 | 1089 | 6.87 |

Table 11: Mechanical parameters of the infill wall.

*Ground motion selection and amplitude modulation.*

Due to the strong uncertainty of ground motions, the input ground motions of incremental dynamic analysis (IDA) must be reasonable. Following the selection principle for ground motion records in FEMA P695 [20], a total of 20 ground motion records were selected, including both far field and nearfield ground motions. Figs. 11 and 12 show the response spectra and mean response spectra of the two types of ground motions, respectively.

The ground motion intensity measure (IM) was characterized by peak ground acceleration (PGA). The amplitude was modulated by the equal step principle. To explore the seismic performance of the infill wall, the amplitude of ground motions was gradually increased to 1.0g with a fixed step size of 0.05g.
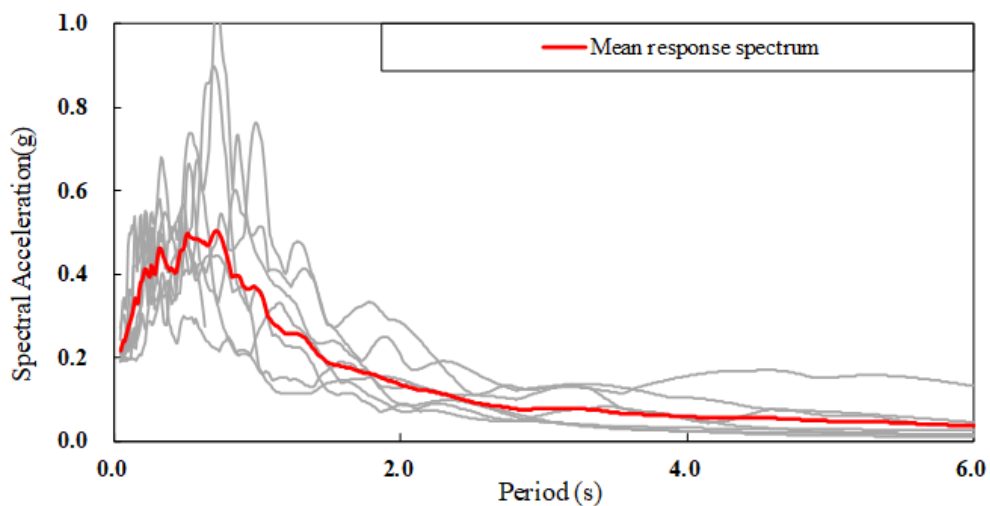


Figure 11: Response spectra and mean response spectra of far field ground motions.
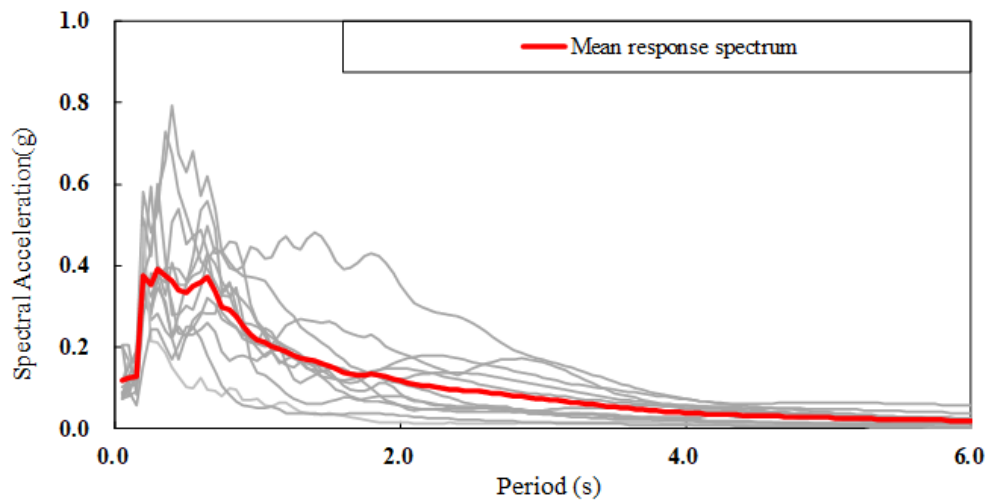
Figure 12: Response spectra and mean response spectra of nearfield ground motions.

## RESULTS AND DISCUSSION

*IDA and vulnerability curves of infill wall.*

Taking the damage indicator measure (DM) of the infill wall as the abscissa, and the PGA as the ordinate, 20 curves were plotted for the IP-OOP infill wall model, and the IP infill wall model, respectively (see the gray curves in Figs. 13 and 14). It can be seen that the IDA curves are directly affected by ground motion records. For the same structure, the responses to different ground motions were, to a certain extent, discrete. To suppress the discreteness of the IDA curves, quantile statistical analysis was performed to draw the IDA curves of the 16%, 50%, and 84% quantiles. Normally, the structural DMs under different IMs all obey log normal distribution. The relationship between IM and DM can be expressed as:

$$DM = \alpha(IM)^{\beta} \tag{18}$$

The logs of IM and DM were subjected to statistical regression to establish a linear regression function. Figs. 15 and 16 report the fitting results of ln(*PGA*)-ln(*DM*).
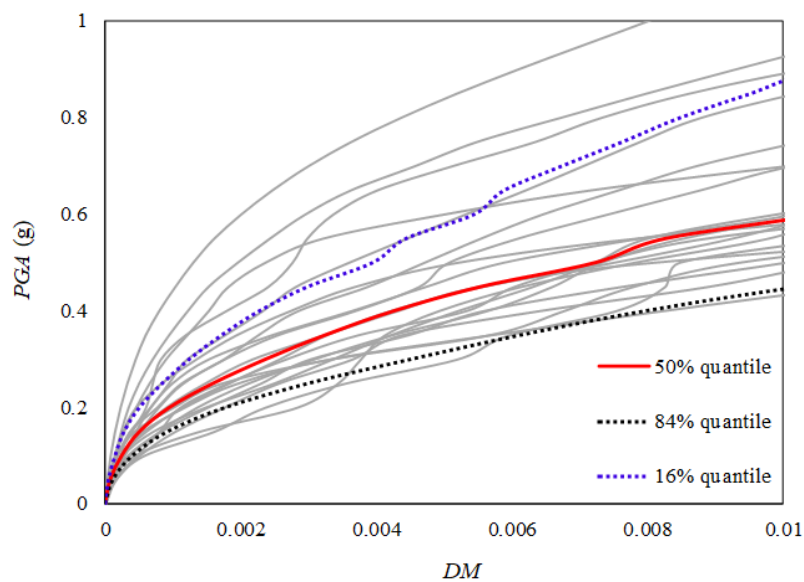


Figure 13: IDA curves of IP-OOP infill wall.
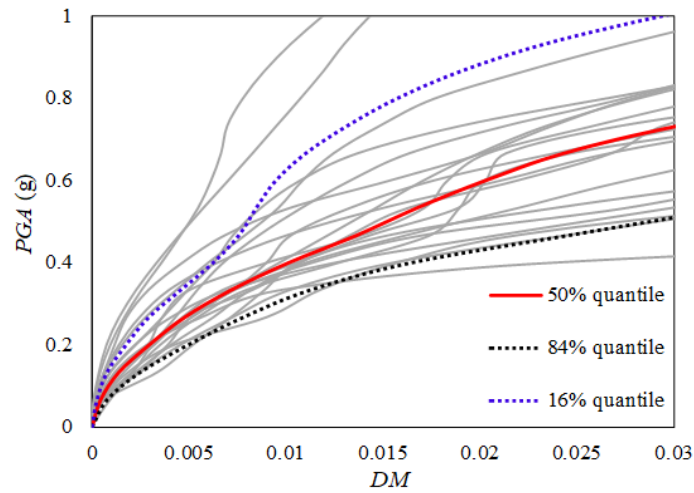
Figure 14: IDA curves of IP infill wall.
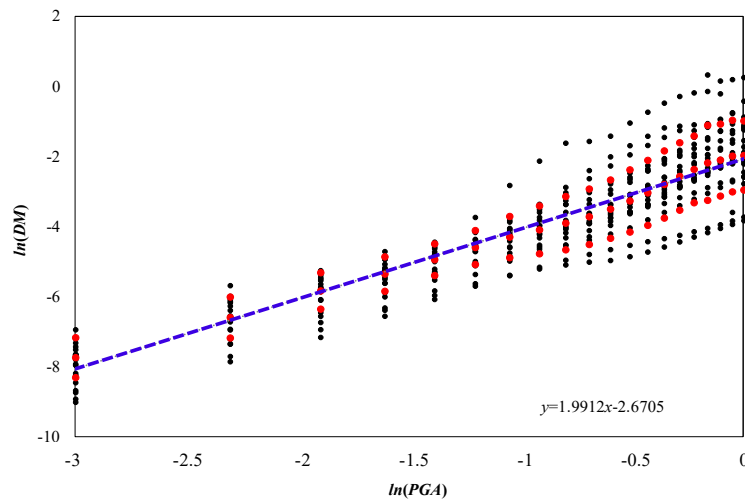


Figure 15: IDA regression results of IP-OOP infill wall.
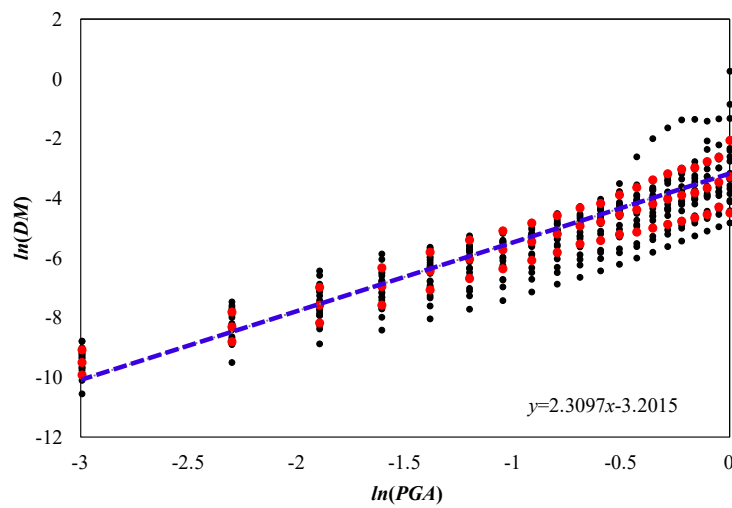


Figure 16: IDA regression results of IP infill wall.

Through the above regression analysis, the probabilistic demand of ground motions for IP-OOP infill wall and IP infill wall can be respectively expressed as:

$$\ln(DM) = 1.9912\ln(PGA) - 2.6705 \tag{19}$$

$$\ln(DM) = 2.3097\ln(PGA) - 3.2015 \tag{20}$$

Under different ground motion intensities, the seismic vulnerability of a structure is the conditional probability for the structural damage indicator to surpass the critical value C for the seismic capacity for the structure defined for the structural damage stage:

$$P_f = P(C / DM < 1) \tag{21}$$

During seismic vulnerability analysis, both the structural DM and the structural capacity parameter C obey log normal distribution. Thus, the structural failure probability can be expressed as:

$$P_f = \Phi\left(-\frac{\ln(C / DM)}{\sqrt{\beta_C^2 + \beta_{DM}^2}}\right) = \Phi\left(\frac{\ln((\alpha(PGA)^\beta)/C)}{\sqrt{\beta_C^2 + \beta_{DM}^2}}\right) \tag{22}$$

where, $P_f$ is the probability for the structural seismic demand to exceed the limit state of seismic capacity; $\alpha$ and $\beta$ are the power exponential relationship coefficients between DM and IM; $C$ is the limit value of structural performance level under different damage states; $\beta_C$ and $\beta_{DM}$ are the log standard deviations obtained through the calculation of structural seismic capacity, and structural seismic demand, respectively.

According to the *Estimated Annualized Earthquake Losses for the United States* (HAZUS 99), $\sqrt{\beta_C^2 + \beta_{DM}^2}$ can be set to 0.5, when the explanatory variable is PGA.

Thus, the failure probability formulas for the IP-OOP infill wall model, and the IP infill wall model can be respectively obtained as:

$$P_f(PGA) = \Phi\left(\frac{\ln\left[\dfrac{0.0692(PGA)^{1.9912}}{C}\right]}{0.5}\right) \tag{23}$$

$$P_f(PGA) = \Phi\left(\frac{\ln\left[\dfrac{0.0408(PGA)^{2.3097}}{C}\right]}{0.5}\right) \tag{24}$$

After computing the exceedance probability of the infill wall under each limit state, the authors compared the vulnerability curves of the two infill wall models under each damage state (Fig. 17). The red solid line and black dotted line are the vulnerability curves of the IP-OOP infill wall model, and the IP infill wall model, respectively. Tab. 12 reports the vulnerability parameters of the two infill walls. Under the same seismic intensity, the infill wall under IP-OOP interactions was more likely to be damaged than that under IP load only.

As shown in Tab. 12 and Fig. 17, the median $\theta$ of the seismic vulnerability function in the IP-OOP infill wall model was lower than that of the function in the IP infill wall model. When the probability of reaching or exceeding DS1 was 50%, the PGAs of the IP-OOP infill wall model, and the IP infill wall model were 0.13g and 0.24g, respectively. When the probability of reaching or exceeding DS2 was 50%, the PGAs of the IP-OOP infill wall model, and the IP infill wall model were0.23g and 0.38g, respectively. When the probability of reaching or exceeding DS3 was 50%, the PGAs of the IP-OOP infill wall model, and the IP infill wall model were0.39g and 0.60g, respectively.

(a) DS1  (b) DS2  (c) DS3
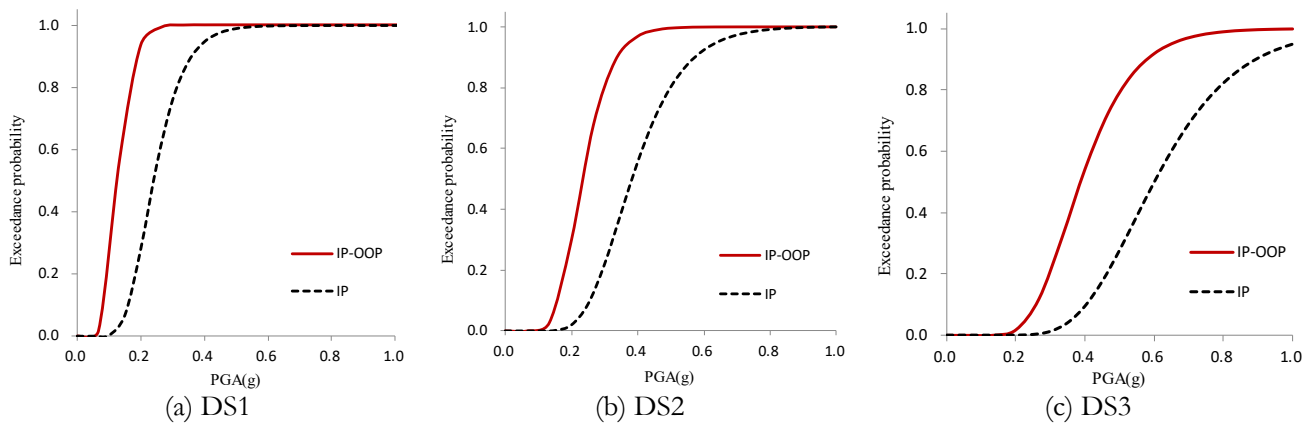
Figure 17: Vulnerability curves of two infill wall models under each damage state.

| Infill wall model | DS1 | | DS2 | | DS3 | |
|---|---|---|---|---|---|---|
| | $\theta(g)$ | $\beta_r$ | $\theta(g)$ | $\beta_r$ | $\theta(g)$ | $\beta_r$ |
| IP-OOP | 0.13 | 0.30 | 0.23 | 0.29 | 0.39 | 0.31 |
| IP | 0.24 | 0.32 | 0.38 | 0.32 | 0.60 | 0.31 |

Table 12: Characteristic parameters of the vulnerability curves of two infill wall models.

For the IP-OOP infill wall, the model was almost certain to suffer slight damage (probability > 90%) when the PGA was 0.15g. For the IP infill wall, the corresponding PGA was 0.27g. For the IP-OOP infill wall, the model was almost certain to suffer moderate damage when the PGA was 0.25g. For the IP infill wall, the corresponding PGA was 0.43g. For the IP-OOP infill wall, the model was almost certain to reach DS3 when the PGA was 0.44g. For the IP infill wall, the corresponding PGA was 0.67g.

The above results show that, for any damage state, the IP-OOP infill wall was always damaged earlier than the IP infill wall. With the rising degree of damage, there was a growing gap between the ground motion intensities required for the two models to reach the same damage state. This phenomenon can be attributed to two possible reasons: Firstly, the performance indicator for the damage state of IP infill wall only considers the IP damages of the wall, failing to take account of the OOP damages. Hence, the bearing capacity of the infill wall is overestimated under seismic effect. Secondly, the effect of IP-OOP interactions mainly manifests as stiffness degradation. The IP damages reduce the OOP stiffness of infill wall. The damaged infill wall has a greater OOP displacement than the intact wall, and is thus more likely to reach the response threshold under the next damage state.

*Damage indicators profiles.*
Figs. 18 and 19 show some typical profiles of the IP indicator and the IP-OOP indicator of infill wall at three different seismic intensities (i.e., 0.1g, 0.2g, 0.4g) during the nonlinear dynamic analyses.
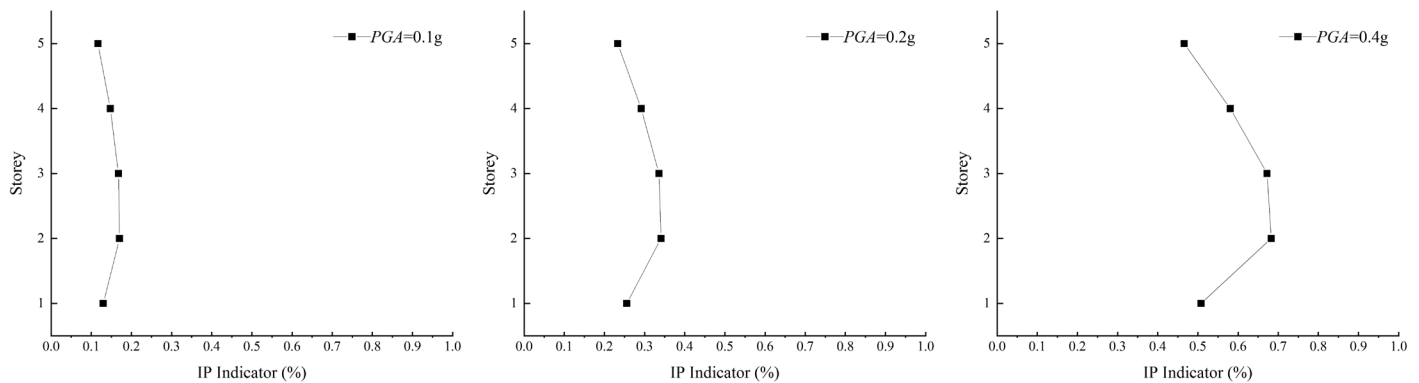


Figure 18: IP indicator profiles of infill wall.
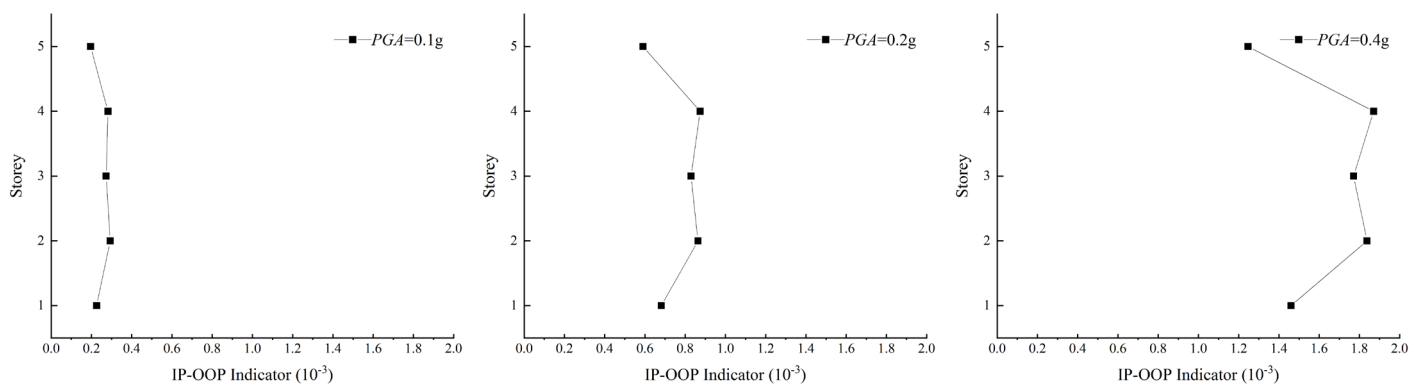
Figure 19: IP-OOP indicator profiles of infill wall.

As can be seen from Figs. 18 and 19, the IP indicator profiles presented a ">" shape, and the IP infill walls had large in-plane deformations at the 2nd and 3rd storeys. The IP infill walls reached or exceeded DS1 and DS2 damage states for the PGA of 0.1g and 0.2g, respectively. At the upper storeys of the structure, the IP indicator values were relatively small, and the infill walls suffered less damage. The vertical variation trend of the IP-OOP indicator showed a "W" shape, and the IP-OOP indicator values were relatively large at the 2nd to 4th storeys of the structure. The IP-OOP infill walls reached or exceeded DS2 and DS3 damage states for the PGA of 0.1g and 0.4g, respectively. Compared with the IP indicator response, the IP-OOP indicator increased significantly at the 4th storey of the structure. It is clearly necessary to consider the IP-OOP interactions of the infill walls under seismic actions, as the increasing OOP suppresses infill wall stiffness. The IP damages of infill walls are proportional to the interlayer displacement angle of the structure, and negatively correlated with the height of the structure. However, the OOP actions on the equivalent elements are proportional to the inertia forces of the infill walls, which generally increase with the height of the structure. Therefore, the effects of IP-OOP interactions on the vulnerability of infill walls can be maximized on the mid-storeys of the structure, and may cause damage to the infill walls in these storeys.

*IDA and vulnerability curves of RC frame with infill wall.*
Taking the maximum interlayer displacement angle as the abscissa, and the PGA as the ordinate, the IDA curves, as well as the IDA curves of the 16%, 50%, and 84% quantiles, were plotted for the frame with IP-OOP infill wall, and the frame with IP infill wall (Figs. 20 and 21).
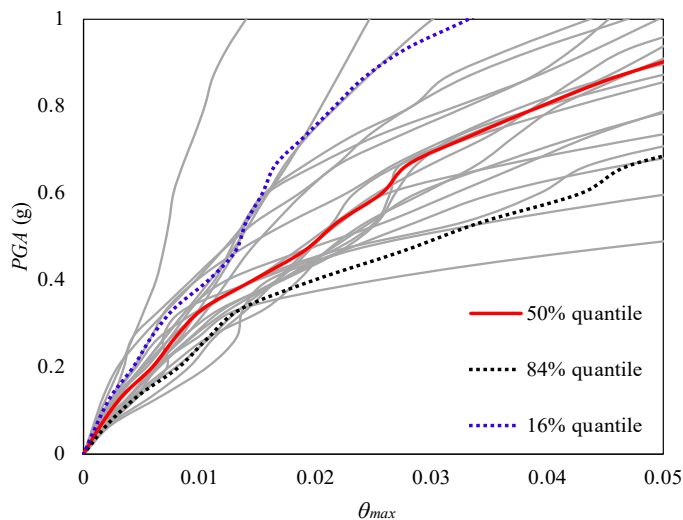


Figure 20: IDA curves of the frame with IP-OOP infill wall.
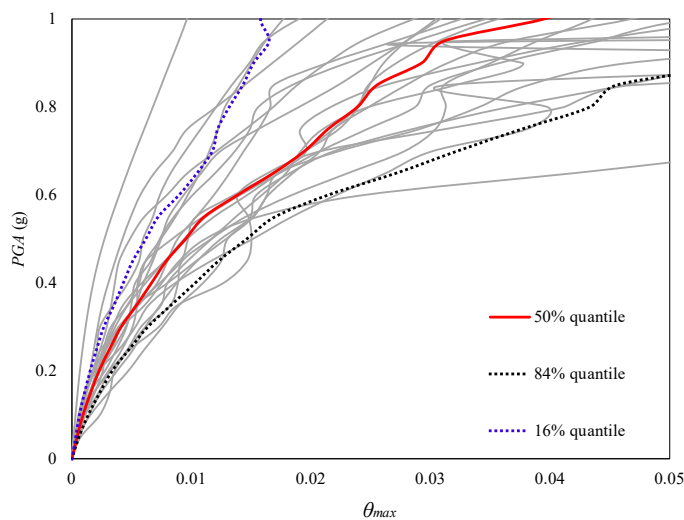


Figure 21: IDA curves of the frame with IP infill wall.

The IDA results show that: for the frame with IP-OOP infill wall, when the PGA was less than 0.3g, the discreteness of the IDA curves was small, the maximum interlayer displacement angle almost changed linearly, and the structure belonged to the elastic stage. When the PGA was greater than 0.3g, the discreteness of the IDA curves gradually increased with a clear nonlinearity, and the structure entered the elastic-plastic stage. Under a rare earthquake (*PGA*=400*gal*), the median of

$\theta_{max}$ was 1.46%, below the limit value of the maximum interlayer displacement angle for partial collapse of the structure. When the PGA was greater than 0.4g, the frame with IP infill wall entered the elastic-plastic stage. Under the ground motions of the same intensity, the frame with infill wall IP-OOP interactions suffered greater lateral deformation than the structure without these interactions. The linear regression results for IDA data are displayed in Figs. 22 and 23.
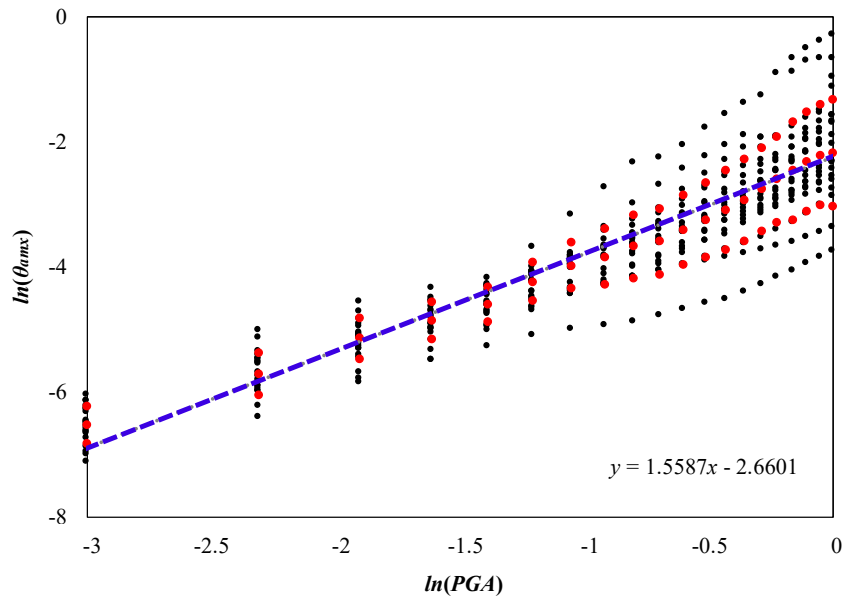


Figure 22: IDA regression results on the frame with IP-OOP infill wall
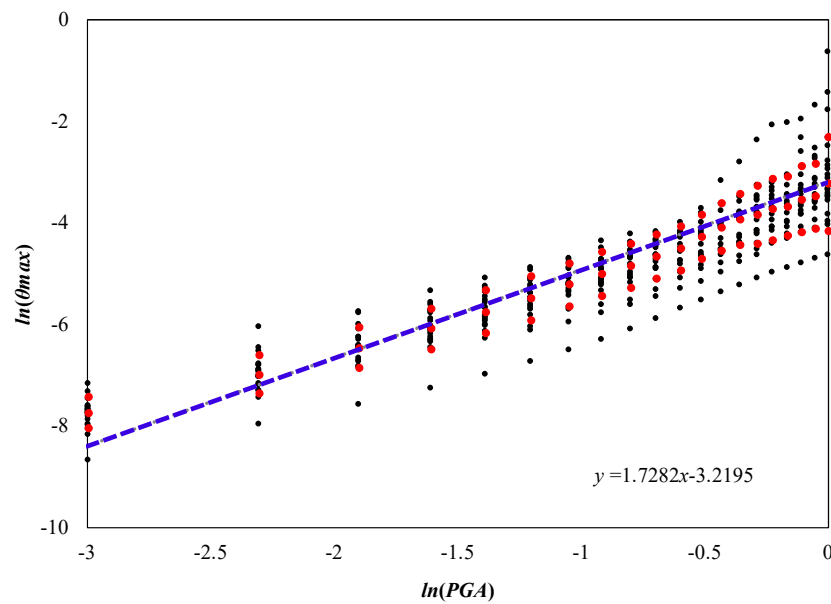


Figure 23: IDA regression results on the frame with IP infill wall

Therefore, the failure probabilities of the frames with IP-OOP and IP infill walls can be respectively calculated by:

$$P_f(PGA) = \left( \frac{\ln\left[ \frac{0.0699(PGA)^{1.5587}}{C} \right]}{0.5} \right) \tag{25}$$

$$P_f(PGA) = \left( \frac{\ln\left[\dfrac{0.0399(PGA)^{1.7282}}{C}\right]}{0.5} \right) \tag{26}$$

Fig. 24 shows the vulnerability curves of the two frames. Tab. 13 lists the characteristic parameters of the vulnerability curves.
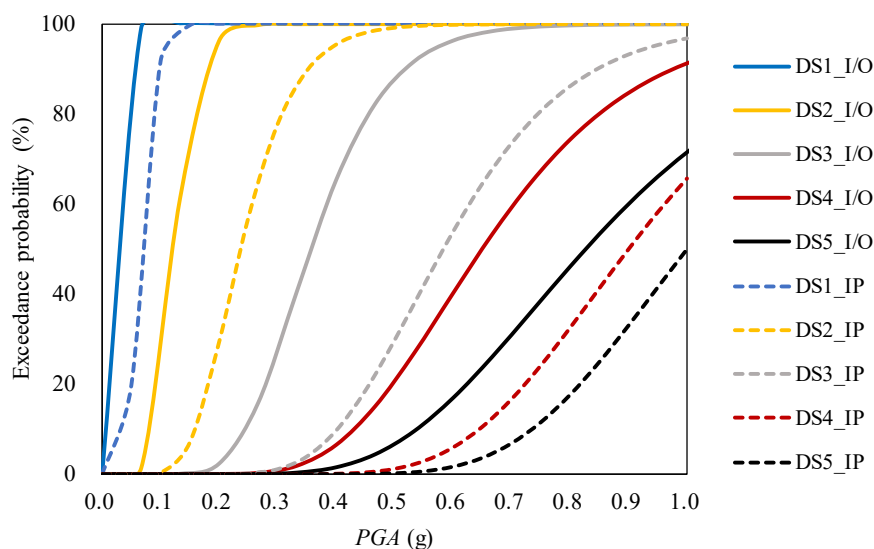


Figure 24: Vulnerability curves of the two frames.

| Vulnerability parameter | | DS1 | DS2 | DS3 | DS4 | DS5 |
|---|---|---|---|---|---|---|
| $\theta$(g) | IP-OOP | 0.03 | 0.12 | 0.36 | 0.65 | 0.83 |
| | IP | 0.07 | 0.24 | 0.58 | 0.90 | 1.00 |
| $\beta_r$ | IP-OOP | 0.30 | 0.27 | 0.29 | 0.32 | 0.34 |
| | IP | 0.31 | 0.31 | 0.29 | 0.26 | 0.24 |

Table 13: Characteristic parameters of the vulnerability curves of the two frames.

Under a frequent earthquake (seismic fortification intensity: 8; 0.20g), the IP-OOP infill wall of the frame was almost certain to have minute cracks ($P(\theta_{max}>0.05\%/PGA=70gal) = 98.95\%$), and the IP infill wall of the frame had a 47.30% likelihood to have minute cracks. Under a moderate earthquake (seismic fortification intensity: 8), the IP-OOP structure was almost certain to face slight damage ($P(\theta_{max}>0.30\%/PGA=200gal) = 96.33\%$), and had a 2.29% likelihood to face moderate damage; the frame of the IP model had a 29.36% likelihood to face moderate damage. Under a rare earthquake (seismic fortification intensity: 8), the frame of the IP model had a 65.37% likelihood to face moderate damage, and was unlikely to approach the partial collapse state ($P(\theta_{max}>2.80\%/PGA=400gal) = 6.46\%$); the frame of the IP model had a very low likelihood (9.57%) to reach the DS3. Both frame models meet the seismic fortification requirements: roughly intact under small earthquakes, repairable under moderation earthquakes, and non-collapsible under strong earthquakes.

Compared with the frame with IP infill wall, the IP-OOP structure had a 51.58% reduction in the likelihood for being intact under a frequent earthquake. Under a moderate earthquake, the probability of slight damage and moderate damage of IP-OOP structure increased by 64.68% and 2.28%, respectively. Under a rare earthquake, the probability of moderate damage and partial collapse of the IP-OOP structure increased by 49.34% and 4.86%, respectively.

As can be seen from the vulnerability curves, the consideration of infill wall IP-OOP interactions can enhance the damage probability of the frame with infill walls. The enhancement was the most significant for the moderate damage to partial

collapse state of the structure. As mentioned in vulnerability curves of infill walls, the infill walls considering IP-OOP interactions were more likely to be damaged under seismic effect than those without considering these interactions. When the frame was moderately damaged, the infill wall in the structure must have been already been severely damaged, and even collapsed. In the IP-OOP model, the equivalent elements of the infill wall were removed after reaching the IP-OOP interaction boundary. The removal may cause vertical non-uniformity and even weak layers in the frame, making the overall structure more likely to collapse. This is a common seismic damage. During seismic vulnerability analysis, the inclusion of IP-OOP interactions of infill walls better reflects the probability for RC frames with infill walls to suffer severe damage and collapse.

## CONCLUSIONS

Based on the infill wall model under IP-OOP interactions, this paper analyzes the seismic vulnerability of RC frames with infill walls through the IDA. The main conclusions are as follows:

(1) According to the 3/2 power curve of the IP and OOP displacements for infill walls, this paper defines an infill wall performance indicator in the light of IP-OOP interactions. The definition and thresholds of the indicator were verified by the data of IP-OOP combined loading tests. The verification results demonstrate the necessity of considering IP-OOP interaction and the accuracy of the indicator.

(2) Through the seismic vulnerability analysis on infill walls, it was learned that, under the same seismic intensity, the infill wall was always more likely to be damaged under IP-OOP interactions than under IP load only. With the growing degree of damage, once the infill wall entered the elastoplastic stage, the vulnerability curve of the infill wall under IP-OOP interactions deviated more and more significantly from that of the infill wall under IP load only. The IP-OOP interactions had the greatest effect on the probability for infill wall to suffer severe damage.

(3) By comparing the damage indicators profiles of infill wall, it was learned that, the IP-OOP interactions could change the trend of the infill wall damage indicators from the bottom to the top of the structure. Its effects on the vulnerability of infill walls could be maximized on the mid storeys of the structure and cause damage to the infill walls in the mid storeys.

(4) Through the seismic vulnerability analysis on RC frames with infill wall, both frame models meet the seismic fortification requirements: largely intact under small earthquakes, repairable under moderation earthquakes, and non-collapsible under strong earthquakes. The infill wall IP-OOP interactions would increase the probability of overall structure damages, especially the probability for moderate to partial collapse states.

According to the previous seismic vulnerability analyses of frames with infill walls, the seismic performance of the overall frame may be improved by considering the IP action of the infill walls. This study discovers that the infill walls and overall structure under IP-OOP interactions were more likely to be damaged than those under infill wall IP effect only. Therefore, the IP-OOP interactions of infill walls should be considered to improve the reasonability of the seismic safety assessment of RC frames with infill walls.

## REFERENCES

[1] Li, J., Xue, Y. and Xiao, C. (2015). Experimental study on seismic performance of full-scale RC frame infilled with autoclaved aerated concrete blocks, J. China Civil Engineering Journal. 48(8), pp. 12-18. DOI: 10.15951/j.tmgcxb.2015.08.002

[2] Xie, X. (2020). The seismic behavior and fragility of masonry infills in reinforced concrete frame structures, Harbin, Institute of Engineering Mechanics, China Earthquake Administration. DOI: 10.27490/d.cnki.ggjgy.2020.000013

[3] Di Domenico, M., Ricci, P. and Verderame, G.M. (2019). Experimental assessment of the out-of-plane strength of URM infill walls with different slenderness and boundary conditions, J. Bulletin of Earthquake Engineering. 17(7), pp. 3959-3993. DOI: 10.1007/s10518-019-00604-5

[4] Furtado, A., Rodrigues, H. and Arête, A. (2016). Experimental evaluation of out-of-plane capacity of masonry infill walls, J. Engineering Structures. 111, pp. 48-63. DOI: 10.1016/j.engstruct.2015.12.013

[5] Gavilán, J.P. (2017). Infill walls with confining elements and horizontal reinforcement: an experimental study, J. Engineering Structures. 150, pp. 153-165. DOI: 10.1016/j.engstruct.2017.07.042

[6] Koutas, L.N. and Bournas, D.A. (2019). Out-of-plane strengthening of masonry-infilled RC frames with textile-reinforced mortar jackets, J. Journal of Composites for Construction. 23(1), pp. 04018079. DOI: 10.1061/(ASCE)CC.1943-5614.0000911

[7] De Risi, M.T., Di Domenico, M. and Ricci, P. (2019). Experimental investigation on the influence of the aspect ratio on the in-plane/out-of-plane interaction for masonry infills in RC frames, J. Engineering Structures. 189, pp. 523-540. DOI: 10.1016/j.engstruct.2019.03.111

[8] Flanagan, R.D. and Bennett, R.M. (1999). Bidirectional behavior of structural clay tile infilled frames, J. Journal of structural engineering. 125(3), pp. 236-244. DOI: 10.1061/(ASCE)0733-9445(1999)125:3(236)

[9] Zhao, W. (2020). Bidirectional seismic performance of infilled RC frames, Yantai, Yantai University. DOI: 10.27437/d.cnki.gytdu.2020.000331

[10] Chiozzi, A. and Miranda, E. (2017). Fragility functions for masonry infill walls with in-plane loading, J. Earthquake Engineering & Structural Dynamics. 46(15), pp. 2831-2850. DOI: 10.1002/eqe.2934

[11] Cardone, D. and Perrone, G. (2015). Developing fragility curves and loss functions for masonry infill walls, J. Earthquakes and Structures. 9(1), pp. 257-279. DOI: 10.12989/eas.2015.9.1.257

[12] Sassun, K., Sullivan, T.J. and Morandi, P. (2016). Characterising the in-plane seismic performance of infill masonry, J. Bulletin of the New Zealand Society for Earthquake Engineering. 49(1), pp. 98-115. DOI: 10.5459/bnzsee.49.1.98-115

[13] Kadysiewski, S. and Mosalam, K.M. (2009). Modeling of unreinforced masonry infill walls considering in-plane and out-of-plane interaction, Berkeley, Pacific Earthquake Engineering Research Center.

[14] Furtado, A., Rodrigues, H. and Arêde, A. (2016). Simplified macro-model for infill masonry walls considering the out-of-plane behaviour, J. Earthquake Engineering & Structural Dynamics. 45(4), pp. 507-524. DOI: 10.1002/eqe.2663

[15] FEMA P-58. (2012). Seismic performance assessment of buildings volume 1: methodology, Washington, D.C, Federal Emergency Management Agency.

[16] Mosalam, K.M. and Günay, S. (2015). Progressive collapse analysis of reinforced concrete frames with unreinforced masonry infill walls considering in-plane/out-of-plane interaction, J. Earthquake Spectra. 31(2), pp. 921-943. DOI: 10.1193/062113EQS165M

[17] Rossetto, T. and Elnashai, A. (2005). A new analytical procedure for the derivation of displacement-based vulnerability curves for populations of RC structures, J. Engineering structures. 27(3), pp. 397-409. DOI: 10.1016/j.engstruct.2004.11.002

[18] Noh, N.M., Liberatore, L. and Mollaioli, F. (2017). Modelling of masonry infilled RC frames subjected to cyclic loads: State of the art review and modelling with OpenSees, J. Engineering Structures. 150, pp. 599-621. DOI: 10.1016/j.engstruct.2017.07.002

[19] Huang, H., Burton, H.V. and Sattar, S. (2020). Development and utilization of a database of infilled frame experiments for numerical modeling, J. Journal of Structural Engineering. 146(6), pp. 04020079. DOI: 10.1061/(ASCE)ST.1943-541X.0002608

[20] FEMA P695. (2009). Quantification of Building Seismic Performance Factors, Washington, D.C, Federal Emergency Management Agency.